

IR-source IRAS 20508+2011: spectral variability of the optical component

V.G. Klochkova¹, V.E. Panchuk¹, N.S. Tavganskaya¹, and G. Zhao²

¹ Special Astrophysical Observatory RAS, Nizhnij Arkhyz, 369167 Russia,

² National Astronomical Observatories CAS, Beijing, China

12th May 2018

Abstract Based on high-resolution spectra we revealed variability of the optical spectrum of the cool star identified with the IR source IRAS 20508+2011. Over the five years of our observations, the radial velocity derived from photospheric absorption lines varied in the interval $V_r = 15 - 30$ km/s. In the same time, the $H\alpha$ profile varied from an intense bell-shaped emission line with a small absorption to 2-peaked emission with a central absorption feature below the continuum level. At all but one epoch, the positions of the metallic photospheric lines were systematically shifted relative to the $H\alpha$ emission: $\Delta V_r = V_r(\text{metal}) - V_r(H, \text{emis}) \approx -23$ km/s. The Na D doublet lines shown a complex profile with broad (half-width ≈ 120 km/s) emission and photospheric absorption, as well as an interstellar component. We used model atmospheres to determine the physical parameters and chemical composition of the star's atmosphere: $T_{\text{eff}}=4800$ K, $\log g=1.5$, $\xi_t=4.0$ km/s and metallicity $[\text{Fe}/\text{H}]=-0.36$. We detected overabundances of oxygen $[\text{O}/\text{Fe}]=+1.79$ (with the ratio $[\text{C}/\text{O}]\approx-0.9$), and α -process elements, as well as a deficit of heavy metals. The totality of the parameters suggests that the optical component of IRAS 20508+2011 is an "O-rich" AGB star with luminosity $M_v \approx -3^m$ that is close to its evolution transition to the post-AGB stage.

1. Introduction

Our program of spectroscopic observations of evolved stars identified with IR sources is being carried out with the 6-m telescope of the Special Astrophysical Observatory of the Russian Academy of Sciences. Its basic goal is to determine the main parameters and evolutionary stages of the stars, search for evolutionary variations of their chemical compositions, study in detail the velocity fields in their atmospheres and envelopes, and detect spectral variability and binarity. The objects under consideration are basically intermediate-mass stars in the asymptotic-giant-branch (AGB) and postAGB stages, which have evolved through stages of hydrogen and helium burning both in the core and layer sources, mixing and ejection of matter, and mass loss via the stellar wind on the AGB. There are strong grounds to expect variable elemental abundances in atmospheres of these evolved objects. Stars in the transition from the AGB to planetary nebulae are conventionally called protoplanetary nebulae (PPN). The main results of the program are briefly summarized by Klochkova et al. [1]. The papers [2], which is the first in our series of works on the spectroscopy of bipolar nebulae, and [3], which presents the first detailed spectroscopic results for the post-AGB object IRAS 01005+7910 are also important. The peculiar spectral variability of this object is apparently due to inhomogeneity of its circumstellar gas-dust envelope. We present here the results of our first spectral observations of the optical component of the IR source IRAS 20508+2011 (hereafter IRAS 20508). The source is beyond the Galactic plane ($b = -15^\circ 3$, $l = 66^\circ 0$), possibly indicating that it does not belong to the young disk population. The IRAS catalog [4] presents the IR fluxes for the source $f_{12}=0.71$, $f_{25}=1.10$, $f_{60}=0.48$, and $f_{100}=1.00$.

Unfortunately, neither multicolor photometric nor spectral data at optical wavelengths that could be used to derive the parameters of the object and reveal its evolutionary status are available. Using the interactive ALADIN atlas from the Strasbourg CDS database, we identified the optical component of IRAS 20508 as the star No. 815697 from the compiled catalog [5], with $B = 12^m 868$ and $V = 11^m 938$ (color index $B-V = 0^m 93$). The star is also present in the catalog GSC HST [6]: No. 0165500558 ($m_{\text{ph}} = 11^m 6$). Detection of strong $H\alpha$ emission in the first spectrum of the star obtained with the 6-m telescope in summer 1999 led us to continue

the observations. In Sect. 2, we give a brief description of our observations and the processing of the spectral data. Sect. 3 describes the features we found in the spectra of the optical component of IRAS 20508, as well as our determination of its chemical composition and the radial velocities in the stellar atmosphere and the circumstellar material.

2. Observations and data reduction

We carried out spectroscopic observations of IRAS 20508 with the 6 m telescope of the SAO. Three spectra were obtained at the prime focus with the PFES echelle spectrograph [7], which provides a spectral resolution of $R \approx 17000$ in combination with a 1160×1040 CCD. The two latest spectra were obtained with the NES echelle spectrograph [8] at the Nasmyth focus, using a 2048×2048 CCD. The NES spectrograph equipped with an image slicer [9] provides a spectral resolution $R = 60000$. Table 1 presents the moments of observations and the wavelength region of the spectra. The data were extracted from the two-dimensional echelle spectra using the ECHELLE procedure in the MIDAS package. Cosmic-ray traces were removed via median averaging of two spectra obtained consecutively. The wavelengths were calibrated using spectra from a Th-Ar hollow-cathode lamp. The further processing, including photometric and position measurements, was carried out with the DECH20 code [10], which enables the determination of positions for individual spectral features by bringing into coincidence the direct and mirror images of their profiles. To increase the accuracy of our radial-velocity measurements, we selected unblended lines for comparisons between observed and synthetic spectra. For each spectrogram, the positional zero point was determined in the standard way, by calibrating based on the positions of ionosphere night sky emission and telluric absorption lines observed against the background of the object's spectrum. The accuracy of the velocity measured from a single line in a spectrum obtained with the PFES spectrograph is about 3.0 km/s; the NES spectrograph provided to measure such single-line velocities with an accuracy of about 1 km/s.

3. Discussion

3.1. Radial velocity pattern of IRAS 20508

In whole the optical spectrum of IRAS 20508 is typical of a late-type supergiant. Fig. 1 compares a part of the observed spectrum with the theoretical spectrum calculated in the LTE-approximation with the model parameters $T_{eff} = 4800$ K, $\log g = 1.5$, and $\xi_t = 4.0$ km/s (the method and accuracy of the model parameters are discussed below, in Subsect. 3.2). No signs of the molecular bands that are often observed in the optical spectra of PPN (see, for example, [1, 11, 12]) are visible in the spectrum of IRAS 20508. The entire set of radial velocities derived from individual lines did not reveal any wavelength dependence of the velocity. Table 2 presents the measurements of the radial velocity V_r for all dates. This table indicates essential time variability of V_r averaged over the lines of metals. At the epoch of our observations, the amplitude of the V_r variations measured from metallic absorption lines is about 15 km/s: $V_r = 15.5 - 29.9$ km/s. Within the uncertainties, the positions of the absorption cores of the $H\beta$ and $H\gamma$ lines whose profiles are not distorted by emission are consistent with the velocity derived from the metallic lines. It follows from Table 2 that the velocity corresponding to the $H\alpha$ emission wings is variable, which may indicate the presence of some disturbing component in the IRAS 20508 system. Further observations are needed to confirm the binarity of the star.

3.1.1. The $H\alpha$ profile variability.

The main feature in the optical spectrum of IRAS 20508 is the intense $H\alpha$ emission (Fig. 2). Since the H profiles in both spectra obtained in 2000 are very similar, only one profile is plotted in Fig. 2 for this year. $H\alpha$ emission is common for stars evolving close to the AGB stage and, along with an IR excess, provides the main criterion for PPN candidates [13]. In the spectra of typical PPN, the $H\alpha$ line displays complex (emission + absorption) variable profiles with core asymmetry, P Cygni or inverse P Cygni profiles, or profiles with asymmetrical emission wings (see, for example, [14, 15]). Such features are also frequently observed in combinations with each other. $H\alpha$ emission is known as a sign of matter outflow and/or pulsations. In the case of PPN, as a rule, the shift of the core is smaller than that corresponding to the escape velocity; i.e., it indicates outflow (expansion) of the upper layers of the extended atmosphere rather than a wind.

Along with the features common for the spectra of stars close to the AGB stage, the $H\alpha$ profile in the spectrum of IRAS 20508 displays its own individual peculiarities, first and foremost extended wings (Fig. 2),

which are uncommon for such a cool supergiant. The $H\alpha$ emission is superimposed with variable absorption, which is systematically shifted by $V_r = V_r(H, abs) - V_r(met) \approx 10$ km/s towards longer wavelengths relative to the photospheric lines (only on the last date of our observations does the position of the H absorption correspond to that of the metallic lines). For all five observing epochs, the intensity of the short-wavelength emission exceeds that of the long-wavelength emission. Over five years of observations, the $H\alpha$ profile in the spectrum of IRAS 20508 varied from an intense, bell-shaped emission feature with only a small amount of core absorption to a two-peak emission line.

It also follows from a comparison of the H profiles in Fig. 2 that the intensity of the emission systematically decreased during 1999–2003; the central absorption line is below the continuum level in the 2003 spectrum. The width of the emission wings of the line also varied. At our first four epochs, when the emission flux decreased systematically relative to the continuum radiation, an essentially constant difference between the radial velocities derived from photospheric absorption lines and the center of gravity of the H emission profile was observed: $V_r = V_r(met) - V_r(H, emis) \approx -23$ km/s. However, the $V_r(met)$ and $V_r(H, emis)$ velocities became virtually equal in the last spectrum obtained in 2004; the $H\alpha$ emission intensity again increased, and the central absorption again exceeded the continuum. Unfortunately, due to the absence of radiospectroscopic observations of IRAS 20508, we cannot determine the systemic velocity of the source or suggest even a preliminary model for the system. Variable $H\alpha$ emission is also a well-known phenomenon for AGB and post-AGB stars [16] (see also references in the present study). Differences in the $H\alpha$ profiles are due to differences in the dynamical processes occurring in the extended atmospheres of these stars, such as spherically symmetrical outflows with a velocity that is either constant or variable with height in the atmosphere, matter falling onto the photosphere, or pulsations. H-profile variability can be naturally explained for a post-AGB star with signs of binarity and mass loss: the $H\alpha$ profile varies due to the orbital motion in the system. However, the $H\alpha$ profiles also vary in those post-AGB objects for which no signs of V_r and brightness variability are detected. The brightness variability may suggest a shock mechanism, like RV Tauri stars, where the dissipation of shocks in the atmosphere probably stimulates matter outflow. The radiative fluxes from AGB and post-AGB stars are insufficient for the radiative wind-generation mechanism, which is efficient in the case of hot massive supergiants. The observed H profile can be considered a combination of two lines with different natures: photospheric absorption and intense emission with a broad set of velocities, forming in a circumstellar structure. In this case, the emission component can be distinguished by subtracting the theoretical photospheric profile from the observed profile. If we subtract the photospheric profile calculated from a model with the solar H/He ratio (indicated in Fig. 3 by the dotted curve), the wings of the resulting emission profile extend to radial velocities of ± 250 km/s.

3.1.2. Structure of the Na D profile.

A detailed study of high-resolution spectra of IRAS 20508 revealed that the Na D resonance doublet also displays a complex profile, with both absorption and emission components. In the spectra obtained with the PFES spectrograph, both the Na D1 and Na D2 lines are unresolved asymmetric blends. Let us consider the spectrum s40402 obtained with high spectral resolution $R \approx 60000$ with the NES spectrograph. Fig. 4 presents the observed spectrum in the area of the Na D doublet, along with the theoretical spectrum and their difference. A comparison of the observed and synthetic spectra shows narrow absorption (indicated by 1 in Fig. 4) and broad emission (indicated by “2” in the difference spectrum in Fig. 4) in the Na D doublet. The position of the emission peak in the Na D doublet lines is roughly consistent with the radial velocity estimated from the absorption lines of metals. The half-width of the narrow absorption feature is a factor of 1.5 smaller than the average half-width of the absorption lines in the spectrum, suggesting that the narrow absorption feature is formed in the interstellar medium. It follows from Table 2 that the velocity of the narrow interstellar component is $V_r = -7.7$ km/s (relative to the Local Standard of Rest, $V_{lsr} = 9.3$ km/s). According to [17], interstellar Na D2 lines at positions corresponding to velocities $V_r \approx -8 \dots -20$ km/s are observed in the Galaxy, in the direction towards the constellation Vulpecula, close to IRAS 20508. Note that, according to [18], the radial velocities of HII regions in the local volume of the Galaxy in the direction towards IRAS 20508 are $V_{lsr, HII} 10$ km/s, which is close to our obtained value. Brand and Blitz [19] presented the velocity $V_{lsr, HII} \approx 21$ km/s ($V_r \approx 5$ km/s) in this same direction, but for a more distant region of the Galaxy with $d = 3.9$ kpc. The presence of a corresponding feature in the spectrum of IRAS 20508 cannot be excluded, in which case, this indicates a larger distance to IRAS 20508, as is also confirmed by the estimated luminosity of the object (see Subsect. 3.2).

The presence of broad (half-widths reaching $V_r \approx 120$ km/s) emission components in the Na D lines suggests that IRAS 20508 belongs to a relatively small group of supergiants with this type of anomaly

in their spectra. Intense and broad (up to 300 km/s) emission in resonance lines, in particular Na D, is observed in the spectrum of R CrB [20] close to its minimum brightness, as well as in the spectrum of FG Sge [21, 22, 23], which manifests itself as a R CrB-type nova, as was shown by Gonzalez et al. [21]. The same spectral peculiarity is also observed for a number of post-AGB stars, for example, 89 Her [23], QY Sge [23], and V510 Pup [12]. In the case of the hotter photosphere of QY Sge, the emission is very strong, far exceeding the continuum level [23]. Rao Kameswara et al. [23] suggest that the resonance-line emission is formed in hot circumstellar envelopes, while the large width results from photon scattering on moving dust particles of the envelope. The Na D emission in the spectrum of IRAS 20508 is distorted by intense absorption forming in the photosphere of the cool supergiant. It is likely that the spectrum of IRAS 20508 displays absorption identified with diffuse interstellar bands (DIB). However, due to the late spectral type of the star, even the strong 5780 Å band is blended by photospheric lines, complicating distinguishing this band and measuring its parameters. For the same reason, the radial velocity is difficult to measure, even for the usually easily discriminated 6613 Å band. In particular, it is blended by the YII line in the spectrum of the cool supergiant.

3.2. Main Parameters of the Star

To determine the basic parameters of the model atmosphere of the star—the effective temperature T_{eff} and gravitational acceleration $\log g$ —and calculate the chemical composition and synthetic spectra, we used the grid of model stellar atmospheres calculated by Kurucz [24] in a hydrostatic approximation for various metallicities. The effective temperature was determined in the usual way, from the condition that the abundance of neutral iron be independent of the excitation potentials for the lines used. The gravitational acceleration was selected based on the condition of ionization balance for the iron atoms, and the microturbulent velocity from the condition that the iron abundance be independent of the line intensities. A supplementary criterion for the reliability of the method is that the same dependence as that for Fe not be derived for other elements represented by numerous lines in the spectra (e.g., Si I, Ca I, Ti I, Cr I, Ni I). In addition, if the microturbulent velocity has been determined with high reliability, there should be no dependence between the individual abundances and equivalent widths of the lines used for the calculation. The abundances of titanium and vanadium derived from lines of neutral atoms and ions are consistent within the uncertainties. This provides evidence that the gravitational acceleration in the atmosphere has been correctly estimated based on the condition that the iron atoms be in ionization balance. Overall, the internal consistency of the parameters suggests that the homogeneous model atmospheres used are adequate for calculations of weak lines in the approximation of LTE. Table 3 presents the elemental abundances (X) for individual lines. Table 4 contains the resulting parameters of the model atmosphere T_{eff} , $\log g$, and ξ_t together with the average elemental abundances relative to iron $[X/\text{Fe}]$. The abundances of elements in the solar photosphere are taken from [25]. The oscillator strengths of spectral lines involved in determination of the model parameters and elemental abundances are given in [26, 27]. The average typical uncertainties in the model parameters for a star with an effective temperature near 5000 K are $T_{\text{eff}} \approx 100$ K, $\log g \approx 0.3$ dex, and $\xi_t \approx 0.5$ km/s. The dispersion of the elemental abundances derived from a set of lines is small: the rms deviation usually does not exceed 0.3 dex (Table 4). All our calculations were carried out using the WIDTH9 code assuming LTE-approach. Corrections for superfine structure and isotopic shifts, which broaden the Ni I, Mn I, and Ba II lines, were not taken into account. To verify the reliability of the derived parameters of the model atmosphere, we compared the observed spectrum with the synthetic spectrum calculated using the STARS code [28]. The observed and theoretical spectra (see example in Fig. 1) are reasonably consistent. When determining the model-atmosphere parameters, we used lines with low and moderate intensity with equivalent widths $W \leq 0.25$ Å, since the approximation of a stationary plane-parallel atmosphere may be inadequate to describe the strongest spectral features. In addition, some strong absorption features may be distorted by the influence of the circumstellar envelope, and if the spectral resolution is not sufficiently high, the intensity of the envelope components will be included in the observed intensities of components formed in the atmosphere. The effective temperature of the central star $T_{\text{eff}}=4800$ K indicates that IRAS 20508 is in the transition from the AGB towards the PPN stage [29]. The value $\log g=1.5$ testifies that the luminosity of the star is not very high. We estimated the absolute magnitude M_v from the equivalent width of the OI 7773 Å oxygen IR triplet, $W=0.57$ Å. It is known that the equivalent width of this triplet $W(\text{OI})$ may represent a good indication of the absolute luminosities of supergiants over a broad interval of temperatures. Using the calibration of Ferro et al. [30], we obtain $M_v \approx -3^m$. Applying the calibration relations of Straižys and Kuriliene [31], we can translate $T_{\text{eff}}=4800$ K and $M_v \approx -3^m$ into the star's spectral class and luminosity type: G5 I–II, which corresponds to the normal color index $(B - V)_o \approx 0.95$, which is consistent with the observed value $B - V=0.93$. We thus conclude that no color excess is observed for the high-latitude

object IRAS 20508. This makes it possible to estimate the distance to the star from its absolute luminosity: $d = V - M_v \approx 10$ kpc. Note here that, according to Neckel and Klare [32], the interstellar absorption in the disk of the Galaxy towards an object with longitude $l = 66^\circ$ is substantial: even at distances up to 1 kpc, the absorption increases to $A_v \geq 3^m$. The absence of any substantial absorption at optical and even UV wavelengths, despite the large amount of dust around the star, is one of the mysteries of PPN. In this sense, the spectral energy distribution (SED) of the supergiant HD 161796=IRAS17436+5003, which displays a strong IR excess [33] and no distortions of the SED at optical and UV wavelengths [34, 35] is considered to be typical. In general, the absence of any substantial absorption at UV wavelengths can be understood if the dust envelope is spatially separated from the central star; thus, the envelope does not substantially affect the radiation of the star. The large distance to IRAS 20508 and the absence of reddening with a large IR excess leads us to consider another aspect of the structure of supergiants with IR excesses and their distances. Menzies and Whitelock [36] noted a paradoxical difference between the distances to the G0I star QY Sge (the optical component of IRAS 20056+1834) obtained using different techniques. Menzies and Whitelock [36] obtained the distance $d \approx 500$ pc for QY Sge based on its interstellar absorption, while taking the absolute magnitude for a population I G0I supergiant to be $M_v = -6^m.5$ yields a distance to QY Sge of $d \approx 36$ kpc (for a low-mass population II supergiant in the post-AGB stage, $d \approx 9$ kpc). To explain this substantial difference, Menzies and Whitelock [36] suggested a model with an extremely inhomogeneous circumstellar envelope heated by the star. QY Sge is considered to be a nearby system ($d \approx 500$ pc), in which the direct radiation from the star towards the observer is obscured by the dust envelope, while the observed flux is determined by scattering on matter ejected by the star earlier and located behind it. In such an aspherical system, the observed flux essentially does not depend on the temperature and luminosity of the star; instead, it is specified by the morphological parameters of the system—the distance between the envelope and central star, the angle between the system’s axis and the line of sight, the angle of the cone in which the star’s radiation emerges, and the optical depth and parameters of the dust particles of the envelope. Similar models were suggested previously for several objects, such as the supergiant VY CMa [37] and the AGB star CIT 3, which is identified with the IR source IRC+1011 [38].

3.3. Chemical abundances pattern

Table 3 presents the measured equivalent widths W for individual lines in one of the spectra (s25309), along with the calculated abundances (X) for the entire set of lines used to determine the chemical composition. We selected this spectrum (s25309) to calculate the chemical composition because it has the highest signal-to-noise ratio (as can be seen in Fig. 1) and a large interval of detected wavelengths. Table 4 presents the averaged abundances for 27 elements. Below, we will analyze in detail the abundances of elements belonging to various groups; first, however, we will consider the separation of elements in the atmosphere of an object with a gas–dust envelope. Separation of elements in the envelope. The studied object may be undergoing a stage of low-intensity mass exchange between the atmosphere and circumstellar gas–dust envelope. However, the very fact that the iron abundance is close to the solar value indicates that condensation on dust particles does not cause any serious distortions in the elemental abundances, since iron is among those elements that most efficiently condense onto particles [39]. The CNO-group elements sulfur and zinc are essentially unaffected by fractioning processes. Since the abundances of CNO elements may vary due to nuclear reactions in the course of the star’s evolution, the behavior of zinc and sulphur is critical for the efficiency of selective separation. The abundance of zinc does not vary in the course of stellar nucleosynthesis in the interiors of low- and medium-mass stars. In combination with the ratio $[Zn/Fe] = -0.24$, which is not appreciably different from its solar value, this suggests that we do not see any selective separation in the circumstellar envelope of IRAS 20508. The abundance of sulfur in the atmosphere of IRAS 20508 is very high: $[S/Fe] = +0.74$. A similar substantial sulfur excess was detected, for example, in the stars HD 331319 = IRAS 19475+3119 and HD 161796 = IRAS 17436+5003 [40], as well as the optical component of the IR source IRAS 04296+3429 [41]. A similar result for sulfur was also obtained for the two evolved stars K 413 [42] and K 307 (a W Vir-type V1 variable) [43], which are members of the globular cluster M 12. Bond and Luck [44] revealed a very large sulfur excess ($[S/Fe] = +1.2$) in the atmosphere of the low-metallicity post-AGB star HD 46703, and suggested that sulfur was synthesized via the capture of particles by ^{12}C nuclei. However, Klochkova [45] also detected an excessive abundance of sulfur in the atmosphere of the normal massive supergiant α Per, which does not have a circumstellar envelope, so that no condensation should be present, while we do not expect the synthesis of sulfur at such an early evolutionary stage. There are grounds to conclude that the sulfur excess is a stable peculiarity in the chemical compositions of evolved stars. Note that this excess is observed in stars with different metallicities and temperatures. Light elements. Let us now consider the

abundances of light metals. No LiI 6707 Å line is seen in the spectrum of IRAS 20508. The abundances of CNO-group elements in its atmosphere are substantially different from the solar values, though these results have only low accuracy. The excess abundance of carbon $[C/Fe] + 0.9$ is determined from four weak CI lines with equivalent widths $W > 10 \text{ mÅ}$. In the case of nitrogen, only the NI 7468 Å line was measured, since the NI 7423 Å line is blended with the SiI line and NI 7442 Å line is beyond the limits of our echelle frame. Therefore, the derived excess of nitrogen should not be considered firm. We calculated the oxygen abundance $[O/Fe] = +1.79$ using reliably measured lines of the OI 7773 Å oxygen IR triplet. However, it is known that the lines of the 7773 Å triplet are sensitive to deviations from LTE. The 7773 Å lines in the spectrum of IRAS 20508 are not very strong, and their total equivalent width is $W = 0.56 \text{ Å}$. Taking into account the calculations of Gratton et al. [46], we can neglect systematic errors in the oxygen abundance derived from the triplet lines assuming LTE for such a cool star, and consider the derived excess to be real. As a result, we obtain $[C/O] = -0.9$ which indicates that IRAS 20508 is a member of the group of evolved objects with oxygenenriched atmospheres. This result is consistent with the position of the object in the *V I b* region in the van der Veen–Habing diagram [47]. Of the even -process elements, we determined the abundances of Mg, Si, Ca, and Ti, in addition to sulfur (see above). The Mg, Ca, and Ti abundances are slightly lower in comparison with the iron abundance; the average excess for these elements is $[X/Fe] = -0.18$. Sodium is overabundant in the atmosphere of IRAS 20508, $[Na/Fe] = +0.58$, which may be due to the synthesis of sodium in the course of hydrogen burning [48, 49]. Some of the derived Na excess is probably due to our failure to take into account superionization of the sodium atoms [50]. The small derived aluminium excess, $[Al/Fe] = +0.32$ is inconsistent with the oxygen excess, as was previously obtained for K 413 [42]: an Al–O anticorrelation [51] is usually observed for evolved stars in globular clusters with average deficits of metals. Iron peak elements. The average abundances of iron-group metals (vanadium, chrom, manganese, cobalt, nickel) differ little from the iron abundance: $[met/Fe] = -0.04$. Individual iron-group elements display no significant deviations towards either over- or underabundances relative to iron. The abundance of copper is slightly low for both stars ($[Cu/Fe] = -0.23$); this value is determined from only two lines, and its significance is fairly low. Heavy metals. It is generally accepted (see, for example, [52]) that the atmospheres of AGB and post-AGB stars may display excesses of heavy metals, due to neutron capture, mixing, and the ejection of matter that has undergone these processes from the stellar interior to its surface. However, in contrast to the expected excess, the atmosphere of the optical component of IRAS 20508 displays a reduced abundance of barium: $[Ba/Fe] \approx -0.4$ (Tables 3, 4). The abundances of the lighter *s*-process metals Y and Zr are also reduced relative to that of iron: $[s/Fe] = -0.28$. The deficit is less severe for the lanthanides La, Ce, Pr, Nd: $[lant/Fe] = -0.11$. A similar weak deficit was obtained for the *r*-process element Eu: $[Eu/Fe] = -0.07$. Deficits of *s*-process elements are observed in the atmospheres of post-AGB stars much more frequently than excesses [1, 14, 45, 53]. It is most likely that the observed absence of any manifestation of the ejection of heavy metals is real, rather than being due to systematic errors in analyses of the spectra of supergiants based on model atmospheres. The presence or absence of an excess of *s*-process elements is probably related to the main parameters of the star, namely, its initial mass and massloss rate, which specify its evolution. Gonzalez and Wallerstein [54] suggest that the basic parameter determining the efficiency of the ejection of the products of nucleosynthesis to surface layers is a star’s luminosity. We have obtained further support for this suggestion, since the luminosity of IRAS 20508 is not very high: $M_v \approx -3^m$.

3.4. Evolutionary status of IRAS 20508

As we noted earlier, according to its the position in the IR color diagram, IRAS 20508 belongs to the *V I b* group in the classification of van der Veen and Habing [47]. This group includes evolved stars, which are often variable and have oxygen-enriched circumstellar envelopes. AGB objects are represented by Mira-type stars, carbon stars, and OH/IR stars. The Miras possess comparatively hot envelopes, are associated with H_2O masers and maser sources radiating mainly in the main *OH* band, and descend from stars that have undergone mass loss at rates below $10^{-5} M_\odot/\text{yr}$ [55]. OH/IR stars are thought to be the final stage of evolution of oxygenrich AGB stars that have undergone mass loss at larger rates (exceeding $10^{-5} M_\odot/\text{yr}$) and are rapidly evolving towards the PPN stage. Unfortunately, no observations in water maser or *OH* bands are available for IRAS 20508, hindering unambiguous classification of the envelope. However, it may be that, in the case of IRAS 20508, we are observing an extremely early phase of PPN formation, immediately after the termination of mass loss and the beginning of the separation of the envelope. Excesses of neither lithium nor *s*-process elements were detected in the atmosphere of IRAS 20508. The mixing that took place in the object is only indicated by the overabundance of *CNO*-group elements, which are products of helium burning. In the case of IRAS 20508, we have obtained further confirmation of the well known corellation [14, 56] between

the C/O ratio and the abundance of s -process elements in the atmospheres of and post-AGB stars. Note also that the parameters of the atmosphere of IRAS 20508, its metallicity, and details of its chemical composition essentially coincide with those for the OH/IR star associated with IRAS 18123+0511 [57].

4. Conclusions

Our high-resolution optical spectroscopic observations made with the 6-m SAO telescope have revealed spectral variability of the cool star with a high absolute luminosity associated with the IR source IRAS 20508+2011. We have identified lines in the spectrum at wavelengths from 4300 to 7930 Å, and measured the equivalent widths and radial velocities of numerous absorption lines of neutral atoms and ions. The radial velocity of the star derived from the photospheric absorption lines is variable: over five years of observations, it varied in the interval 15–30 km/s. Over the same time, the $H\alpha$ absorption-emission profile also varied substantially: a bell-shaped emission line with only a small amount of core absorption was transformed into a two-peak emission feature with central absorption below the continuum. Further observations with higher spectral resolution are required to explain this variability. The NaD doublet lines also display a complex profile that consists of broad (with half-width 120 km/s) emission, whose position corresponds to that of photospheric absorption lines in the spectrum, and narrow absorption with an interstellar origin. The derived parameters of the star (its luminosity, effective temperature $T_{eff} = 4800$ K, gravitational acceleration $\log g = 1.5$, microturbulent velocity $\xi_t = 4.0$ km/s, and metallicity $[Fe/H] = -0.36$) indicate that the optical component of IRAS 20508+2011 is a star that is close to the AGB stage with an absolute magnitude of $M_v - 3^m$ at a distance of $d \approx 10$ kpc.

The chemical composition of its atmosphere is fairly usual for this evolutionary stage. The relation between the carbon excess $[C/Fe] \approx +0.9$ and oxygen excess $[O/Fe] = +1.79$ suggests that IRAS 20508 is a member of the group of evolved stars with oxygen-enriched atmospheres ($[C/O] = -0.9$), consistent with its position in the IR colour diagram. No excess of s -process elements is observed, which correlates well with the low absolute luminosity of the star and the ratio of its carbon and oxygen abundances, $[C/O]$.

5. Acknowledgements

This work was supported by the Russian Foundation for Basic Research (project No. 03-02-39019), the Basic Research Program of the Department of Physical Sciences of the Russian Academy of Sciences “Extended Objects in the Universe” (“Spectroscopy of Extended Envelopes of Stars in Late Stages of Their Evolution”), and the grant from the National Science Foundation of China (No. 10433010). This publication is based on work supported by Award No. RUP1-2687-NA-05 of the U.S. Civilian Research & Development Foundation (CRDF). This research has used the SIMBAD database and ALADIN interactive sky atlas of the Strasbourg Center for Astronomical Data (CDS).

References

1. V.G.Klochkova, V.E.Panchuk, and R.Szczerba. *Astrophys. Space Sci.*, **265**, 265 (2001).
2. V.G.Klochkova, V.E.Panchuk, M.V.Yushkin, and A.S.Miroshnichenko. *Astron. Rep.*, **48**, 288 (2004).
3. V.G.Klochkova, M.V.Yushkin, A. S. Miroshnichenko, et al. *A&A*, **392**, 143 (2002).
4. Infrared Astronomical Satellite Catalogs. 1988. The Point Source Catalog, Version 2.0. NASA RP-1190. Joint IRAS Working Group (1988).
5. N.V.Kharchenko. *Kin. & Fiz. Neb. Tel*, **17**, 409 (2001).
6. J.E.Morrison, S.Roeser, B.McLean, et al. *Astron. J.*, **121**, 1752 (2001).
7. V.E.Panchuk, I.D.Naidenov, V.G.Klochkova, et al. *Bull. Spec. Astrophys. Observ.*, **44**, 127 (1998).
8. V.E.Panchuk, N.E.Piskunov, V.G.Klochkova, et al. Preprint SAO No. 169, (2002).
9. V.E.Panchuk, M.V.Yushkin, I.D.Naidenov. Preprint SAO No. 179, (2003).
10. G.A.Galazutdinov. Preprint SAO No. 92, (1992).
11. E.J.Bakker, E.F. van Dishoeck, L.B.F.M.Waters, and T.Schoenmaker. *A&A*, **323**, 469 (1997).
12. V.G.Klochkova and E.L.Chentsov. *Astron. Rep.*, **48**, 301 (2004).
13. S.Kwok. *Ann. Rev. A&A*, **31**, 63 (1993).
14. V.G.Klochkova. *Bull. Spec. Astrophys. Observ.*, **44**, 5 (1998).
15. T.Maas, H. van Winckel, and T. Lloyd Evans. *A&A*, **429**, 297 (2005).
16. R.D.Oudmaijer and E.J.Bakker. *MNRAS*, **271**, 615 (1994).
17. L.M.Hobbs. *ApJ Suppl.*, **38**, 129 (1978).
18. Y.P.Georgelin and Y.M.Georgelin. *A&A*, **6**, 349 (1970).
19. J.Brand and L.Blitz. *A&A*, **275**, 67 (1993).
20. N.Rao Kameswara, D.L.Lambert, M.A.Adams, et al. *MNRAS*, **310**, 717 (1999).
21. G.Gonzalez, D.L.Lambert, G. Wallerstein, et al. *ApJ Suppl.*, **114**, 133 (1998).
22. T.Kipper, V.G.Klochkova. *Inf. Bull. Var. Stars*, No. 4661 (1999).
23. N.Rao Kameswara, A.Goswami, and D.L.Lambert. *MNRAS*, **334**, 129 (2002).
24. R.L.Kurucz. CD-ROMs Smithsonian Astrophys. Observ., Cambridge. (1993).
25. N.Grevesse, A.Noels, and A.J.Sauval. *Astron. Soc. Pac. Conf. Ser.*, **99**, 117 (1996).
26. V.G.Klochkova and V.E.Panchuk. *Bull. Spec. Astrophys. Observ.*, **41**, 5 (1996).
27. V.G.Klochkova, P.Szczerba, and V.E.Panchuk. *Astron. Lett.*, **26**, 439 (2000).
28. V.Tsymbal. In: *Model Atmospheres and Spectrum Synthesis*, Eds. S.J.Adelman, F.Kupka, and W.W.Weiss. *Astron. Soc. Pac. Conf. Ser.* **108**, 198 (1996).
29. D.Schönberner. *ApJ*, **272**, 708 (1983).
30. A.Arellano Ferro, S.Giridhar, and E.Rojo Arellano. *Rev. Mex. Astron. Astrofis.*, **39**, 3 (2003).
31. V.Straižys and G.Kuriliene. *Astrophys. Space Sci.* **80**, 353 (1981).
32. Th.Neckel and G.Klare. *Bull. Am. Astron. Soc.*, **42**, 251, (1980).
33. M.Parthasarathy and S.R.Pottash. *A&A*, **154**, 16 (1986).
34. R.M.Humphreys and E.P.Ney. *ApJ*, **190**, 339 (1974).
35. M.Parthasarathy, S.R.Pottash, W.Wamsteker. *A&A*, **203**, 117 (1988).
36. J.W.Menzies and P.A.Whitelock. *MNRAS*, **233**, 697 (1988).
37. G.H.Herbig. *ApJ*, **162**, 557 (1970).
38. D.Vinković, T.Blöcker, K.-H.Hofmann, et al. *MNRAS*, **352**, 852 (2004).
39. H.E.Bond. *Nature*, **356**, 474 (1992).
40. V.G.Klochkova, V.E.Panchuk, N.S.Tavolganskaya. *Astron. Lett.*, **28**, 49 (2002).
41. V.G.Klochkova, R.Szczerba, V. E.Panchuk, and K.Volk. *A&A*, **345**, 905 (1999).
42. V.G.Klochkova, N.N.Samus. *A&A*, **378**, 455 (2001).
43. V.G.Klochkova, V.E.Panchuk, N.S.Tavolganskaya, V.V.Kovtyukh. *Astron. Lett.*, **29**, 748 (2003).
44. H.E.Bond, R.E.Luck. *ApJ*, **312**, 203 (1987).
45. V.G.Klochkova. *MNRAS*, **272**, 710 (1995).
46. R.G.Gratton, E.Caretta, K.Eriksson, B.Gustafsson. *A&A*, **350**, 955 (1999).
47. W.C.E.J. van der Veen, H.J.Habing. *A&A*, **194**, 125 (1998).
48. P.A.Denisikov, V.V.Ivanov. *Sov. Astron. Lett.*, **13**, 214 (1987).
49. P.A.Denisikov. *Sov. Astron. Lett.* **14**, 435 (1988).
50. L.I.Mashonkina, V.V.Shimanskii, N.A.Sakhibullin. *Astron. Rep.*, **44**, 790 (2000).
51. M.D.Shetrone. *Astron. J.*, **112**, 1517 (1996).
52. T.Blöcker. *Astrophys. Space Sci.*, **275**, 1 (2001).
53. H. van Winckel. *Astron. Astrophys. Rev.*, **41**, 391 (2003).
54. G.Gonzalez and G.Wallerstein. *Astron. J.*, **108**, 1325 (1994).
55. B.M.Lewis. *ApJ*, **338**, 234 (1989).
56. V.V.Smith, D.L.Lambert. *ApJ Suppl.*, **72**, 387 (1990).
57. V.G.Klochkova, G.Zhao, P.E.Panchuk, N.S.Tavolganskaya. *Astron. Rep.*, **45**, 553 (2001).

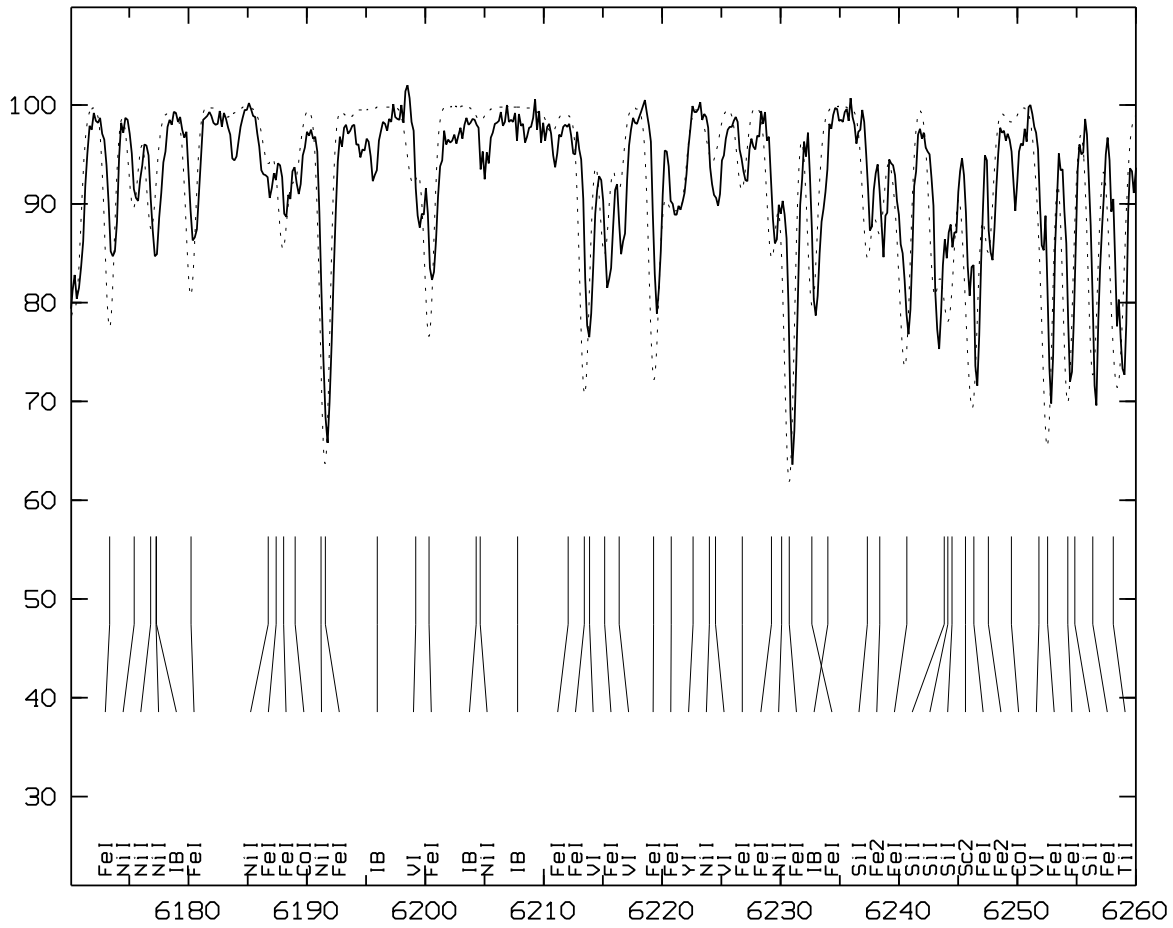


Figure 1. Fragment of the observed spectrum of IRAS 20508+2011 (solid) and the theoretical spectrum (dashed) calculated with the model parameters $T_{eff}=4800$ K, $\log g=1.5$, $\xi_t=4.0$ km/s.

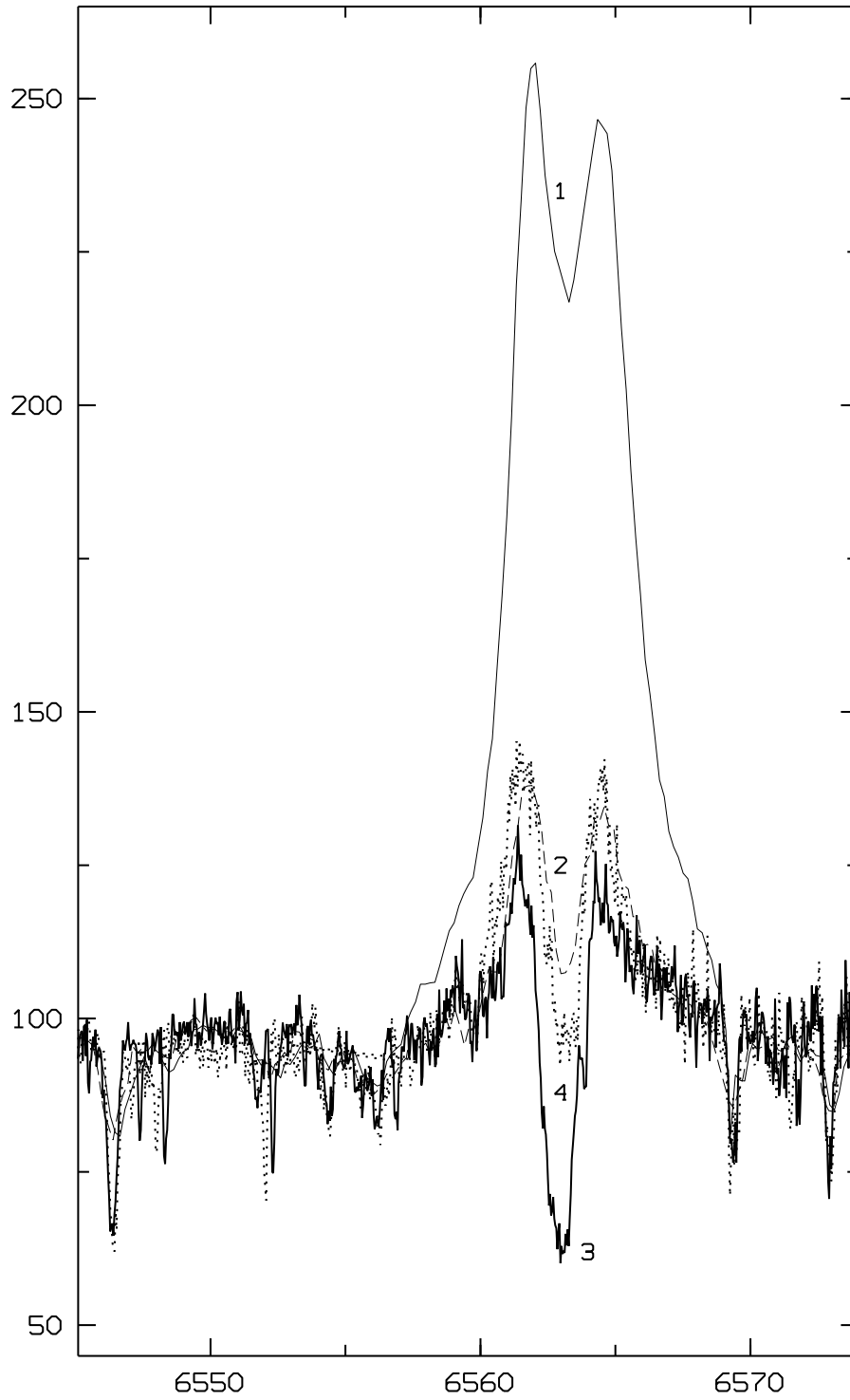


Figure 2. $H\alpha$ profile in spectra of IRAS 20508+2011 obtained in (1) 1999, (2) 2000, (3) 2003, and (4) 2004.

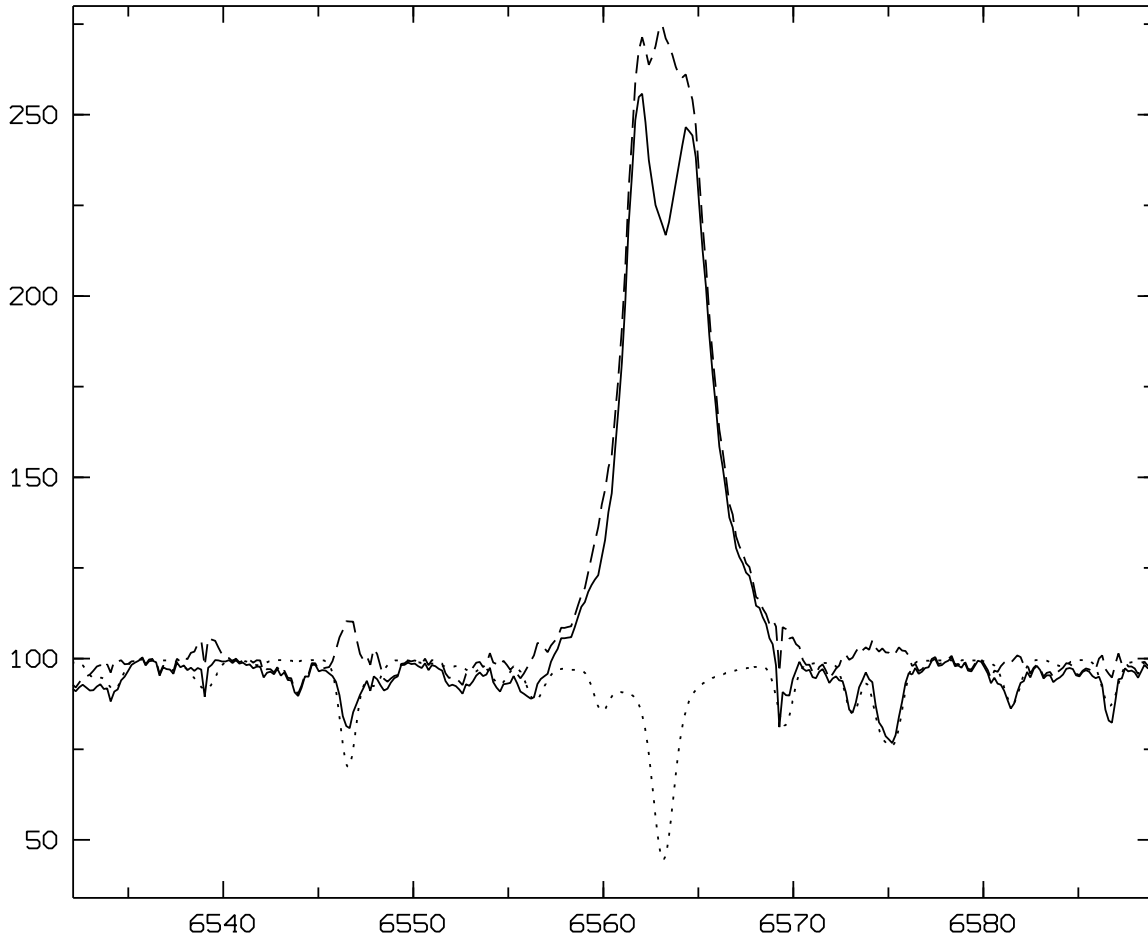


Figure 3. $H\alpha$ line profile in spectrum s25309 of IRAS 20508+2011 (solid) together with the theoretical spectrum (dotted). The dashed curve indicates the difference between the observed and theoretical spectra.

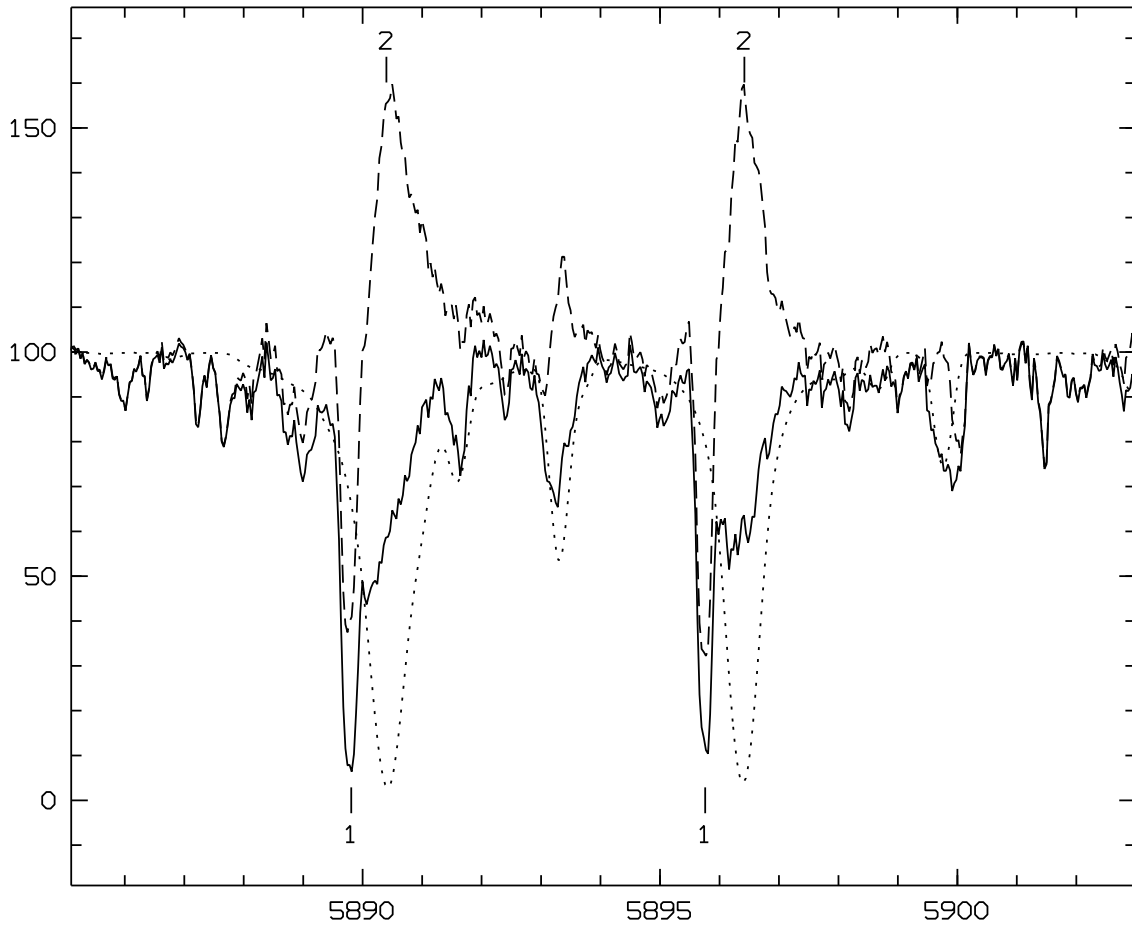


Figure 4. Same as Fig. 3 for the Na D line in spectrum s40402. Figures “1” and “2” indicate the positions of narrow absorption and broad emission features (see the text).

Table 1. Observations of IRAS 20508+2011 with the 6 m telescope

| Spectrum | Date | UT | $\Delta\lambda$, Å | Spectrograph |
|----------|------------|-------|---------------------|--------------|
| s25309 | 28.07.1999 | 21:50 | 4550–7930 | PFES |
| s28208 | 04.07.2000 | 23:13 | 4300–7820 | PFES |
| s28412 | 06.07.2000 | 23:35 | 4320–7825 | PFES |
| s40402 | 10.08.2003 | 23:05 | 5270–6760 | NES |
| s43223 | 27.08.2004 | 22:51 | 5270–6760 | NES |

Table 2. Mean heliocentric radial velocities for line groups and some individual lines derived from IRAS 20508+2011 spectra obtained on various dates. Uncertain values are given by *Italic*.

| Spectral features | $V_{r\odot}$, km/s | | | | |
|----------------------|---------------------|----------|-------------|-----------|----------|
| | 28.07.99 | 04.07.00 | 06.07.00 | 10.08.03. | 27.08.04 |
| <u>Absorptions</u> | | | | | |
| metals | 15.5 | 29.8 | 27.1 | 20.3 | 29.9 |
| H α | 23.1 | 38.6 | 40.7 | 21.4 | 38.0 |
| H β | 16.5 | 27.0 | 24.4 | | |
| H γ | | 27.6 | 23.7 | | |
| <u>Emission</u> | | | | | |
| H α | 39.3 | 51.6 | <i>57.1</i> | 43.1 | 27.0 |
| I.S. NaI(D1,D2) | -4.6 | -5.9 | -5.5 | -7.7 | -7.3 |

Table 3. Lines identification and their intensities in spectrum s25309 of IRAS 20508+2011 and the elemental abundances derived

| λ , Å | Ion | EP, eV | gf | W_{λ} , mÅ | $\epsilon(X)$ |
|---------------|-----|--------|-------|--------------------|---------------|
| 6014.84 | Cl | 8.64 | -1.71 | 13 | -3.00 |
| 6671.82 | Cl | 8.85 | -1.65 | 16 | -2.69 |
| 7100.30 | Cl | 8.64 | -1.60 | 19 | -2.81 |
| 7115.19 | Cl | 8.64 | -0.90 | 29 | -3.23 |
| 7468.31 | NI | 10.34 | -0.13 | 27 | -2.67 |
| 7771.94 | OI | 9.15 | 0.33 | 210 | -1.73 |
| 7774.17 | OI | 9.15 | 0.19 | 214 | -1.48 |
| 7775.39 | OI | 9.15 | -0.03 | 147 | -1.91 |
| 4668.57 | NaI | 2.10 | -1.25 | 161 | -5.40 |
| 4751.83 | NaI | 2.10 | -2.10 | 91 | -5.19 |
| 5682.65 | NaI | 2.10 | -0.71 | 229 | -5.42 |
| 4703.00 | MgI | 4.34 | -0.38 | 268 | -5.20 |
| 5711.10 | MgI | 4.34 | -1.68 | 136 | -5.28 |
| 7657.61 | MgI | 5.11 | -1.28 | 134 | -4.90 |
| 6696.03 | AlI | 3.14 | -1.32 | 136 | -5.48 |
| 7835.32 | AlI | 4.02 | -0.47 | 113 | -5.53 |
| 7836.13 | AlI | 4.02 | -0.29 | 116 | -5.69 |
| 5665.56 | SiI | 4.92 | -2.04 | 42 | -5.06 |
| 5684.49 | SiI | 4.95 | -1.65 | 142 | -4.46 |
| 5690.43 | SiI | 4.93 | -1.87 | 64 | -4.96 |
| 5772.15 | SiI | 5.08 | -1.75 | 100 | -4.58 |
| 5793.08 | SiI | 4.93 | -2.06 | 83 | -4.59 |
| 5948.55 | SiI | 5.08 | -1.23 | 160 | -4.57 |
| 6087.79 | SiI | 5.87 | -1.71 | 20 | -4.72 |
| 6125.03 | SiI | 5.61 | -1.51 | 55 | -4.67 |
| 6145.02 | SiI | 5.61 | -1.48 | 43 | -4.84 |
| 6237.33 | SiI | 5.61 | -1.14 | 92 | -4.67 |
| 6721.84 | SiI | 5.56 | -1.26 | 63 | -4.90 |
| 7034.91 | SiI | 5.87 | -0.88 | 61 | -4.96 |
| 7405.79 | SiI | 5.61 | -0.54 | 150 | -4.80 |
| 7800.00 | SiI | 6.18 | -0.71 | 101 | -4.42 |
| 6347.09 | SiI | 8.12 | 0.26 | 61 | -4.48 |
| 5696.63 | SI | 7.87 | -1.21 | 16 | -4.15 |
| 6045.99 | SI | 7.87 | -0.79 | 18 | -4.47 |
| 6052.63 | SI | 7.87 | -0.63 | 16 | -4.69 |
| 6743.58 | SI | 7.87 | -0.70 | 43 | -3.93 |
| 6757.16 | SI | 7.87 | -0.29 | 22 | -4.81 |
| 5261.71 | CaI | 2.52 | -0.58 | 174 | -6.30 |
| 5349.47 | CaI | 2.71 | -0.31 | 214 | -5.96 |
| 5581.98 | CaI | 2.52 | -0.56 | 223 | -5.88 |
| 5588.76 | CaI | 2.52 | 0.36 | 284 | -6.19 |
| 5590.13 | CaI | 2.52 | -0.57 | 232 | -5.78 |
| 5594.47 | CaI | 2.52 | 0.10 | 291 | -5.87 |
| 5598.49 | CaI | 2.52 | -0.09 | 277 | -5.82 |
| 5601.29 | CaI | 2.52 | -0.52 | 218 | -5.98 |
| 5867.57 | CaI | 2.93 | -1.79 | 67 | -5.60 |

| λ , Å | Ion | EP, eV | gf | W_λ , mÅ | $\epsilon(X)$ |
|---------------|------|--------|-------|------------------|---------------|
| 6162.18 | CaI | 1.90 | -0.09 | 369 | -6.01 |
| 6166.44 | CaI | 2.52 | -1.14 | 114 | -6.35 |
| 6439.08 | CaI | 2.52 | 0.39 | 321 | -6.09 |
| 6471.67 | CaI | 2.52 | -0.69 | 219 | -5.93 |
| 6499.65 | CaI | 2.52 | -0.82 | 208 | -5.89 |
| 6508.84 | CaI | 2.53 | -2.65 | 27 | -5.75 |
| 6572.80 | CaI | 0.00 | -4.31 | 145 | -6.07 |
| 6717.69 | CaI | 2.71 | -0.52 | 251 | -5.60 |
| 7202.21 | CaI | 2.71 | -0.26 | 212 | -6.25 |
| 5239.81 | ScII | 1.45 | -0.77 | 129 | -9.60 |
| 5357.19 | ScII | 1.51 | -2.21 | 23 | -9.27 |
| 5526.79 | ScII | 1.77 | 0.13 | 170 | -9.77 |
| 5669.04 | ScII | 1.50 | -1.09 | 109 | -9.43 |
| 6245.62 | ScII | 1.51 | -0.93 | 151 | -9.26 |
| 6320.84 | ScII | 1.50 | -1.71 | 56 | -9.34 |
| 6604.58 | ScII | 1.36 | -1.48 | 120 | -9.18 |
| 5009.65 | TiI | 0.02 | -2.20 | 147 | -7.48 |
| 5020.03 | TiI | 0.84 | -0.36 | 190 | -7.90 |
| 5038.40 | TiI | 1.43 | 0.07 | 197 | -7.50 |
| 5043.58 | TiI | 0.84 | -1.68 | 117 | -7.21 |
| 5147.48 | TiI | 0.00 | -1.96 | 157 | -7.69 |
| 5194.04 | TiI | 2.10 | -0.50 | 52 | -7.44 |
| 5201.10 | TiI | 2.09 | -0.69 | 42 | -7.38 |
| 5338.33 | TiI | 0.83 | -1.81 | 44 | -7.77 |
| 5426.26 | TiI | 0.02 | -2.95 | 44 | -7.64 |
| 5460.50 | TiI | 0.05 | -2.75 | 85 | -7.42 |
| 5490.15 | TiI | 1.46 | -0.88 | 107 | -7.37 |
| 5514.54 | TiI | 1.44 | -0.50 | 100 | -7.83 |
| 5644.14 | TiI | 2.27 | 0.00 | 103 | -7.31 |
| 5689.47 | TiI | 2.30 | -0.41 | 50 | -7.36 |
| 5716.45 | TiI | 2.30 | -0.64 | 16 | -7.70 |
| 5739.46 | TiI | 2.25 | -0.54 | 29 | -7.57 |
| 5739.98 | TiI | 2.24 | -0.61 | 54 | -7.19 |
| 5766.33 | TiI | 3.29 | 0.31 | 29 | -7.20 |
| 5774.04 | TiI | 3.31 | 0.54 | 26 | -7.46 |
| 5839.76 | TiI | 1.46 | -2.36 | 06 | -7.43 |
| 5866.45 | TiI | 1.07 | -0.78 | 117 | -7.92 |
| 5903.32 | TiI | 1.07 | -2.09 | 46 | -7.22 |
| 5922.11 | TiI | 1.05 | -1.41 | 115 | -7.33 |
| 5937.81 | TiI | 1.07 | -1.83 | 65 | -7.29 |
| 5944.68 | TiI | 0.00 | -3.79 | 14 | -7.43 |
| 5965.83 | TiI | 1.88 | -0.35 | 100 | -7.49 |
| 5978.54 | TiI | 1.87 | -0.44 | 92 | -7.47 |
| 5988.56 | TiI | 1.89 | -1.12 | 46 | -7.20 |
| 6064.63 | TiI | 1.05 | -1.89 | 65 | -7.26 |
| 6126.22 | TiI | 1.07 | -1.37 | 68 | -7.73 |
| 6258.10 | TiI | 1.44 | -0.30 | 133 | -7.85 |
| 6261.10 | TiI | 1.43 | -0.42 | 147 | -7.64 |
| 6303.75 | TiI | 1.44 | -1.51 | 42 | -7.41 |
| 6743.12 | TiI | 0.90 | -1.57 | 87 | -7.63 |

| λ , Å | Ion | EP, eV | gf | W_λ , mÅ | $\epsilon(X)$ |
|---------------|------|--------|-------|------------------|---------------|
| 7138.91 | TiI | 1.44 | -1.53 | 51 | -7.35 |
| 4708.65 | TiII | 1.24 | -2.21 | 137 | -7.90 |
| 4779.98 | TiII | 2.05 | -1.37 | 152 | -7.67 |
| 5185.90 | TiII | 1.89 | -1.35 | 149 | -7.92 |
| 5211.53 | TiII | 2.59 | -1.85 | 88 | -7.21 |
| 5336.78 | TiII | 1.58 | -1.70 | 172 | -7.73 |
| 5381.01 | TiII | 1.57 | -2.08 | 161 | -7.50 |
| 5418.80 | TiII | 1.58 | -2.17 | 131 | -7.67 |
| 6606.97 | TiII | 2.06 | -2.79 | 44 | -7.38 |
| 5670.85 | VI | 1.08 | -0.42 | 42 | -8.91 |
| 5703.59 | VI | 1.05 | -0.21 | 72 | -8.86 |
| 5727.05 | VI | 1.08 | -0.01 | 126 | -8.60 |
| 5727.65 | VI | 1.05 | -0.87 | 79 | -8.14 |
| 5737.06 | VI | 1.06 | -0.74 | 73 | -8.30 |
| 5830.68 | VI | 3.11 | 0.62 | 10 | -8.23 |
| 6039.73 | VI | 1.06 | -0.65 | 78 | -8.37 |
| 6090.21 | VI | 1.08 | -0.06 | 98 | -8.79 |
| 6119.53 | VI | 1.06 | -0.32 | 69 | -8.79 |
| 6150.16 | VI | 0.30 | -1.78 | 65 | -8.31 |
| 6199.19 | VI | 0.29 | -1.30 | 100 | -8.54 |
| 6216.37 | VI | 0.28 | -1.29 | 130 | -8.36 |
| 6251.82 | VI | 0.29 | -1.34 | 94 | -8.55 |
| 6266.32 | VI | 0.28 | -2.29 | 40 | -8.12 |
| 6274.65 | VI | 0.27 | -1.67 | 35 | -8.81 |
| 6285.16 | VI | 0.28 | -1.51 | 48 | -8.80 |
| 6504.16 | VI | 1.18 | -1.23 | 39 | -8.08 |
| 5819.93 | VII | 2.52 | -1.70 | 18 | -8.50 |
| 6028.27 | VII | 2.49 | -1.98 | 22 | -8.16 |
| 6029.00 | VII | 2.56 | -1.94 | 09 | -8.55 |
| 5214.14 | CrI | 3.37 | -0.74 | 38 | -6.68 |
| 5221.76 | CrI | 3.38 | -0.57 | 51 | -6.68 |
| 5238.97 | CrI | 2.71 | -1.30 | 77 | -6.48 |
| 5272.01 | CrI | 3.45 | -0.42 | 71 | -6.55 |
| 5300.74 | CrI | 0.98 | -2.12 | 240 | -6.34 |
| 5304.19 | CrI | 3.46 | -0.69 | 45 | -6.54 |
| 5312.88 | CrI | 3.45 | -0.56 | 82 | -6.31 |
| 5628.64 | CrI | 3.42 | -0.77 | 58 | -6.38 |
| 5783.11 | CrI | 3.32 | -0.50 | 101 | -6.38 |
| 5783.89 | CrI | 3.32 | -0.29 | 116 | -6.47 |
| 6501.20 | CrI | 0.98 | -3.66 | 56 | -6.49 |
| 6630.00 | CrI | 1.03 | -3.56 | 32 | -6.84 |
| 6680.15 | CrI | 4.16 | -0.52 | 32 | -6.15 |
| 6789.15 | CrI | 3.84 | -1.17 | 14 | -6.27 |
| 6925.22 | CrI | 3.45 | -0.33 | 92 | -6.54 |
| 6979.81 | CrI | 3.46 | -0.41 | 114 | -6.27 |
| 5237.35 | CrII | 4.07 | -1.16 | 89 | -7.07 |
| 5308.46 | CrII | 4.07 | -1.81 | 101 | -6.29 |
| 5310.73 | CrII | 4.07 | -2.28 | 56 | -6.32 |
| 5313.61 | CrII | 4.07 | -1.65 | 63 | -6.87 |
| 5334.88 | CrII | 4.07 | -1.89 | 63 | -6.62 |

| λ , Å | Ion | EP, eV | gf | W_λ , mÅ | $\epsilon(X)$ |
|---------------|------|--------|-------|------------------|---------------|
| 5508.63 | CrII | 4.16 | -2.11 | 59 | -6.36 |
| 5394.68 | MnI | 0.00 | -3.50 | 179 | -7.59 |
| 5399.47 | MnI | 3.85 | -0.64 | 20 | -7.28 |
| 5407.43 | MnI | 2.14 | -1.74 | 161 | -6.79 |
| 5420.37 | MnI | 2.14 | -1.46 | 186 | -6.84 |
| 5432.56 | MnI | 0.00 | -3.80 | 150 | -7.52 |
| 5457.47 | MnI | 2.16 | -2.76 | 39 | -6.82 |
| 5516.78 | MnI | 2.18 | -1.85 | 122 | -6.96 |
| 5537.76 | MnI | 2.19 | -2.21 | 36 | -7.39 |
| 6013.48 | MnI | 3.07 | -0.25 | 167 | -7.14 |
| 6016.64 | MnI | 3.07 | -0.24 | 153 | -7.27 |
| 6021.79 | MnI | 3.08 | 0.03 | 144 | -7.61 |
| 6440.93 | MnI | 3.77 | -1.52 | 06 | -7.10 |
| 5002.79 | FeI | 3.40 | -1.58 | 206 | -4.63 |
| 5028.13 | FeI | 3.57 | -1.10 | 218 | -4.75 |
| 5044.21 | FeI | 2.85 | -2.15 | 161 | -5.19 |
| 5054.64 | FeI | 3.64 | -2.14 | 89 | -4.89 |
| 5133.69 | FeI | 4.18 | 0.14 | 230 | -5.17 |
| 5141.74 | FeI | 2.42 | -2.15 | 242 | -4.90 |
| 5162.27 | FeI | 4.18 | 0.02 | 224 | -5.13 |
| 5228.41 | FeI | 4.22 | -1.29 | 153 | -4.51 |
| 5236.19 | FeI | 4.19 | -1.72 | 97 | -4.62 |
| 5243.78 | FeI | 4.26 | -1.15 | 123 | -4.88 |
| 5281.79 | FeI | 3.04 | -1.02 | 247 | -5.26 |
| 5288.53 | FeI | 3.69 | -1.67 | 139 | -4.89 |
| 5293.97 | FeI | 4.14 | -1.87 | 96 | -4.53 |
| 5302.30 | FeI | 3.28 | -0.88 | 250 | -5.06 |
| 5315.07 | FeI | 4.37 | -1.55 | 97 | -4.58 |
| 5321.11 | FeI | 4.43 | -1.44 | 98 | -4.61 |
| 5322.04 | FeI | 2.28 | -3.03 | 145 | -5.19 |
| 5329.99 | FeI | 4.08 | -1.30 | 139 | -4.81 |
| 5358.12 | FeI | 3.30 | -3.37 | 25 | -4.82 |
| 5364.87 | FeI | 4.45 | 0.22 | 223 | -5.04 |
| 5365.40 | FeI | 3.57 | -1.28 | 175 | -5.09 |
| 5373.71 | FeI | 4.47 | -0.86 | 91 | -5.20 |
| 5379.57 | FeI | 3.69 | -1.48 | 119 | -5.26 |
| 5383.37 | FeI | 4.31 | 0.50 | 241 | -5.30 |
| 5386.34 | FeI | 4.15 | -1.77 | 40 | -5.19 |
| 5391.46 | FeI | 4.15 | -0.94 | 175 | -4.74 |
| 5398.29 | FeI | 4.45 | -0.67 | 112 | -5.25 |
| 5400.50 | FeI | 4.37 | -0.16 | 202 | -4.98 |
| 5410.91 | FeI | 4.47 | 0.28 | 225 | -5.06 |
| 5417.03 | FeI | 4.42 | -1.68 | 34 | -5.07 |
| 5441.32 | FeI | 4.31 | -1.73 | 63 | -4.79 |
| 5445.04 | FeI | 4.39 | -0.02 | 203 | -5.11 |
| 5452.12 | FeI | 3.64 | -2.86 | 51 | -4.57 |
| 5464.29 | FeI | 4.14 | -1.72 | 86 | -4.78 |
| 5522.46 | FeI | 4.21 | -1.55 | 49 | -5.24 |
| 5536.59 | FeI | 2.83 | -3.81 | 12 | -5.29 |
| 5543.15 | FeI | 3.69 | -1.57 | 168 | -4.74 |

| λ , Å | Ion | EP, eV | gf | W_λ , mÅ | $\epsilon(X)$ |
|---------------|-----|--------|-------|------------------|---------------|
| 5543.94 | FeI | 4.22 | -1.14 | 126 | -4.93 |
| 5554.89 | FeI | 4.55 | -0.44 | 188 | -4.66 |
| 5557.95 | FeI | 4.47 | -1.28 | 122 | -4.53 |
| 5560.23 | FeI | 4.43 | -1.19 | 106 | -4.80 |
| 5563.60 | FeI | 4.19 | -0.99 | 158 | -4.83 |
| 5565.71 | FeI | 4.61 | -0.29 | 178 | -4.84 |
| 5567.40 | FeI | 2.61 | -2.80 | 141 | -5.09 |
| 5618.65 | FeI | 4.21 | -1.38 | 129 | -4.68 |
| 5633.97 | FeI | 4.99 | -0.27 | 131 | -4.85 |
| 5635.85 | FeI | 4.26 | -1.89 | 66 | -4.67 |
| 5638.27 | FeI | 4.22 | -0.87 | 124 | -5.23 |
| 5652.32 | FeI | 4.26 | -1.95 | 43 | -4.86 |
| 5653.89 | FeI | 4.39 | -1.64 | 55 | -4.89 |
| 5679.02 | FeI | 4.65 | -0.92 | 107 | -4.81 |
| 5686.53 | FeI | 4.55 | -0.63 | 166 | -4.70 |
| 5717.85 | FeI | 4.28 | -1.13 | 116 | -4.96 |
| 5720.89 | FeI | 4.55 | -1.95 | 40 | -4.57 |
| 5738.22 | FeI | 4.22 | -2.34 | 42 | -4.54 |
| 5741.86 | FeI | 4.26 | -1.73 | 51 | -5.00 |
| 5752.04 | FeI | 4.55 | -0.99 | 77 | -5.14 |
| 5753.12 | FeI | 4.26 | -0.76 | 183 | -4.75 |
| 5775.09 | FeI | 4.22 | -1.23 | 94 | -5.13 |
| 5778.47 | FeI | 2.59 | -3.59 | 76 | -4.86 |
| 5793.93 | FeI | 4.22 | -1.70 | 41 | -5.19 |
| 5806.73 | FeI | 4.61 | -1.05 | 124 | -4.60 |
| 5807.79 | FeI | 3.29 | -3.41 | 39 | -4.60 |
| 5809.25 | FeI | 3.88 | -1.84 | 103 | -4.84 |
| 5826.64 | FeI | 4.28 | -2.94 | 06 | -4.80 |
| 5827.89 | FeI | 3.28 | -3.41 | 41 | -4.58 |
| 5833.93 | FeI | 2.61 | -3.66 | 54 | -4.98 |
| 5852.19 | FeI | 4.55 | -1.33 | 103 | -4.57 |
| 5855.13 | FeI | 4.61 | -1.76 | 52 | -4.55 |
| 5856.08 | FeI | 4.29 | -1.64 | 71 | -4.84 |
| 5859.61 | FeI | 4.55 | -0.60 | 167 | -4.73 |
| 5862.36 | FeI | 4.55 | -0.38 | 132 | -5.27 |
| 5873.21 | FeI | 4.26 | -2.14 | 53 | -4.57 |
| 5883.84 | FeI | 3.96 | -1.36 | 170 | -4.66 |
| 5902.52 | FeI | 4.59 | -1.81 | 23 | -4.95 |
| 5916.25 | FeI | 2.45 | -2.99 | 180 | -4.80 |
| 5927.80 | FeI | 4.65 | -1.09 | 95 | -4.76 |
| 5930.17 | FeI | 4.65 | -0.23 | 205 | -4.62 |
| 5934.66 | FeI | 3.93 | -1.17 | 128 | -5.26 |
| 5952.75 | FeI | 3.98 | -1.44 | 93 | -5.21 |
| 5984.80 | FeI | 4.73 | -0.31 | 180 | -4.69 |
| 5987.06 | FeI | 4.79 | -0.59 | 137 | -4.72 |
| 6003.03 | FeI | 3.88 | -1.12 | 140 | -5.27 |
| 6020.17 | FeI | 4.61 | -0.27 | 193 | -4.75 |
| 6024.07 | FeI | 4.55 | -0.12 | 159 | -5.30 |
| 6055.99 | FeI | 4.73 | -0.46 | 112 | -5.17 |
| 6082.72 | FeI | 2.22 | -3.57 | 140 | -4.85 |

| λ , Å | Ion | EP, eV | gf | W_λ , mÅ | $\epsilon(X)$ |
|---------------|-----|--------|-------|------------------|---------------|
| 6094.42 | FeI | 4.65 | -1.94 | 35 | -4.55 |
| 6096.69 | FeI | 3.98 | -1.93 | 83 | -4.82 |
| 6105.15 | FeI | 4.55 | -2.05 | 18 | -4.89 |
| 6127.91 | FeI | 4.14 | -1.69 | 93 | -4.79 |
| 6157.73 | FeI | 4.08 | -1.26 | 132 | -4.97 |
| 6180.22 | FeI | 2.73 | -2.78 | 129 | -5.12 |
| 6188.04 | FeI | 3.94 | -1.72 | 87 | -5.05 |
| 6200.32 | FeI | 2.61 | -2.44 | 181 | -5.17 |
| 6213.43 | FeI | 2.22 | -2.66 | 210 | -5.20 |
| 6215.15 | FeI | 4.19 | -1.44 | 150 | -4.51 |
| 6226.77 | FeI | 3.88 | -2.22 | 63 | -4.84 |
| 6229.23 | FeI | 2.85 | -2.97 | 108 | -4.95 |
| 6232.64 | FeI | 3.65 | -1.33 | 175 | -5.04 |
| 6246.32 | FeI | 3.60 | -0.96 | 244 | -4.84 |
| 6254.26 | FeI | 2.28 | -2.48 | 249 | -4.96 |
| 6271.29 | FeI | 3.33 | -2.95 | 90 | -4.53 |
| 6301.50 | FeI | 3.65 | -0.59 | 241 | -5.20 |
| 6311.51 | FeI | 2.83 | -3.23 | 67 | -5.05 |
| 6336.84 | FeI | 3.69 | -1.05 | 239 | -4.72 |
| 6353.84 | FeI | 0.91 | -6.48 | 17 | -4.85 |
| 6355.04 | FeI | 2.85 | -2.42 | 177 | -4.96 |
| 6380.75 | FeI | 4.19 | -1.40 | 112 | -4.88 |
| 6392.55 | FeI | 2.28 | -4.03 | 71 | -4.89 |
| 6408.02 | FeI | 3.69 | -1.00 | 221 | -4.94 |
| 6411.65 | FeI | 3.65 | -0.82 | 211 | -5.25 |
| 6419.98 | FeI | 4.73 | -0.24 | 145 | -5.11 |
| 6518.38 | FeI | 2.83 | -2.75 | 173 | -4.69 |
| 6581.22 | FeI | 1.49 | -4.86 | 139 | -4.54 |
| 6593.88 | FeI | 2.43 | -2.42 | 206 | -5.25 |
| 6597.61 | FeI | 4.80 | -1.07 | 90 | -4.69 |
| 6608.03 | FeI | 2.28 | -4.03 | 41 | -5.21 |
| 6609.12 | FeI | 2.56 | -2.69 | 185 | -5.01 |
| 6627.56 | FeI | 4.55 | -1.68 | 60 | -4.65 |
| 6646.98 | FeI | 2.61 | -3.99 | 50 | -4.75 |
| 6653.88 | FeI | 4.15 | -2.52 | 26 | -4.72 |
| 6703.57 | FeI | 2.76 | -3.16 | 112 | -4.86 |
| 6705.10 | FeI | 4.61 | -1.28 | 98 | -4.64 |
| 6710.31 | FeI | 1.49 | -4.88 | 95 | -4.84 |
| 6715.41 | FeI | 4.61 | -1.64 | 51 | -4.72 |
| 6726.67 | FeI | 4.61 | -1.12 | 114 | -4.67 |
| 6733.16 | FeI | 4.64 | -1.58 | 42 | -4.86 |
| 6737.98 | FeI | 4.56 | -1.75 | 59 | -4.58 |
| 6739.54 | FeI | 1.56 | -4.95 | 54 | -5.04 |
| 6750.15 | FeI | 2.42 | -2.62 | 189 | -5.22 |
| 6752.72 | FeI | 4.64 | -1.36 | 63 | -4.84 |
| 6806.85 | FeI | 2.73 | -3.21 | 110 | -4.87 |
| 6810.28 | FeI | 4.61 | -1.12 | 86 | -4.91 |
| 6837.00 | FeI | 4.59 | -1.81 | 28 | -4.90 |
| 6843.67 | FeI | 4.55 | -0.93 | 108 | -4.98 |
| 6855.16 | FeI | 4.56 | -0.63 | 172 | -4.72 |

| λ , Å | Ion | EP, eV | gf | W_λ , mÅ | $\epsilon(X)$ |
|---------------|------|--------|-------|------------------|---------------|
| 6858.16 | FeI | 4.61 | -1.06 | 80 | -5.02 |
| 5132.66 | FeII | 2.81 | -4.18 | 103 | -4.53 |
| 5197.56 | FeII | 3.23 | -2.10 | 213 | -4.95 |
| 5534.83 | FeII | 3.24 | -2.93 | 111 | -5.20 |
| 5991.37 | FeII | 3.15 | -3.74 | 114 | -4.48 |
| 6084.10 | FeII | 3.20 | -3.98 | 55 | -4.81 |
| 6113.33 | FeII | 3.22 | -4.31 | 38 | -4.69 |
| 6149.25 | FeII | 3.89 | -2.92 | 89 | -4.71 |
| 6238.38 | FeII | 3.89 | -2.87 | 118 | -4.47 |
| 6247.55 | FeII | 3.89 | -2.51 | 126 | -4.73 |
| 6369.46 | FeII | 2.89 | -4.36 | 39 | -4.99 |
| 6383.72 | FeII | 5.55 | -2.27 | 10 | -4.95 |
| 6416.92 | FeII | 3.89 | -2.85 | 56 | -5.16 |
| 6432.68 | FeII | 2.89 | -3.74 | 90 | -5.03 |
| 7479.69 | FeII | 3.89 | -3.88 | 11 | -5.05 |
| 7711.71 | FeII | 3.90 | -2.74 | 91 | -4.89 |
| 5212.70 | CoI | 3.51 | -0.11 | 76 | -7.33 |
| 5342.71 | CoI | 4.02 | 0.36 | 81 | -7.17 |
| 5352.05 | CoI | 3.58 | 0.06 | 73 | -7.46 |
| 5359.20 | CoI | 4.15 | -0.09 | 19 | -7.38 |
| 5523.30 | CoI | 2.33 | -1.85 | 34 | -7.48 |
| 5530.78 | CoI | 1.71 | -2.06 | 80 | -7.53 |
| 5647.23 | CoI | 2.28 | -1.56 | 34 | -7.84 |
| 6249.50 | CoI | 2.04 | -2.41 | 69 | -6.92 |
| 6632.44 | CoI | 2.28 | -2.00 | 62 | -7.14 |
| 6814.95 | CoI | 1.95 | -1.90 | 125 | -7.14 |
| 5010.96 | NiI | 3.63 | -0.87 | 105 | -6.29 |
| 5017.58 | NiI | 3.54 | -0.08 | 186 | -6.41 |
| 5032.75 | NiI | 3.90 | -1.27 | 34 | -6.33 |
| 5035.37 | NiI | 3.63 | 0.29 | 208 | -6.43 |
| 5084.08 | NiI | 3.68 | 0.03 | 184 | -6.38 |
| 5094.42 | NiI | 3.83 | -1.08 | 63 | -6.25 |
| 5102.97 | NiI | 1.68 | -2.62 | 159 | -6.43 |
| 5155.77 | NiI | 3.90 | -0.09 | 163 | -6.24 |
| 5176.57 | NiI | 3.90 | -0.44 | 102 | -6.46 |
| 5578.72 | NiI | 1.68 | -2.64 | 179 | -6.31 |
| 5847.00 | NiI | 1.68 | -3.21 | 81 | -6.55 |
| 6086.29 | NiI | 4.27 | -0.53 | 85 | -6.13 |
| 6175.42 | NiI | 4.09 | -0.53 | 90 | -6.30 |
| 6327.60 | NiI | 1.68 | -3.15 | 90 | -6.59 |
| 6378.26 | NiI | 4.15 | -0.89 | 64 | -6.12 |
| 6586.33 | NiI | 1.95 | -2.81 | 135 | -6.26 |
| 6643.64 | NiI | 1.68 | -2.30 | 175 | -6.82 |
| 6767.77 | NiI | 1.83 | -2.17 | 168 | -6.82 |
| 6772.36 | NiI | 3.66 | -0.98 | 83 | -6.45 |
| 7110.91 | NiI | 1.93 | -2.98 | 111 | -6.33 |
| 7122.24 | NiI | 3.54 | 0.04 | 253 | -6.19 |
| 5105.55 | CuI | 1.39 | -1.51 | 203 | -8.57 |
| 5218.21 | CuI | 3.82 | 0.27 | 120 | -8.20 |
| 4722.16 | ZnI | 4.03 | -0.39 | 138 | -8.02 |

| λ , Å | Ion | EP, eV | gf | W_{λ} , mÅ | $\epsilon(X)$ |
|---------------|------|--------|-------|--------------------|---------------|
| 4810.54 | ZnI | 4.08 | -0.17 | 158 | -7.98 |
| 5630.14 | YI | 1.36 | 0.15 | 07 | -10.01 |
| 6023.41 | YI | 0.00 | -1.85 | 04 | -10.05 |
| 6222.61 | YI | 0.00 | -1.69 | 02 | -10.43 |
| 6687.50 | YI | 0.00 | -0.43 | 17 | -10.76 |
| 5087.42 | YII | 1.08 | -0.17 | 139 | -10.70 |
| 5200.41 | YII | 0.99 | -0.57 | 139 | -10.42 |
| 5289.82 | YII | 1.03 | -1.85 | 28 | -10.24 |
| 5728.89 | YII | 1.84 | -1.12 | 24 | -10.14 |
| 5853.67 | BaII | 0.60 | -1.00 | 186 | -10.68 |
| 6141.71 | BaII | 0.70 | -0.08 | 270 | -10.74 |
| 6496.90 | BaII | 0.60 | -0.38 | 299 | -10.39 |
| 6262.25 | LaII | 0.40 | -1.45 | 43 | -10.93 |
| 6320.41 | LaII | 0.17 | -1.42 | 32 | -11.39 |
| 6390.48 | LaII | 0.32 | -1.49 | 23 | -11.31 |
| 5330.58 | CeII | 0.86 | -0.23 | 27 | -11.05 |
| 5610.24 | CeII | 1.04 | 0.00 | 49 | -10.76 |
| 6043.38 | CeII | 1.20 | -0.17 | 08 | -11.32 |
| 5219.03 | PrII | 0.79 | -0.24 | 09 | -11.95 |
| 5322.82 | PrII | 0.48 | -0.54 | 24 | -11.55 |
| 5234.21 | NdII | 0.55 | -0.33 | 92 | -10.84 |
| 5293.17 | NdII | 0.82 | -0.06 | 122 | -10.53 |
| 5311.48 | NdII | 0.99 | -0.42 | 26 | -11.00 |
| 5485.71 | NdII | 1.26 | -0.12 | 38 | -10.79 |
| 5740.88 | NdII | 1.16 | -0.55 | 11 | -11.10 |
| 5842.39 | NdII | 1.28 | -0.60 | 08 | -11.05 |
| 6031.31 | NdII | 1.28 | -0.70 | 17 | -10.62 |
| 6437.64 | EuII | 1.32 | -0.28 | 15 | -11.82 |
| 6645.13 | EuII | 1.38 | 0.20 | 24 | -12.01 |

Table 4. Chemical composition $\log \epsilon(X)$ ($\log \epsilon(H) = 12.0$); “n” means the number of lines used, σ – the dispersion of the derived abundance for the given number of lines; model parameters are indicated under the spectrum number; abundances in the solar photosphere are taken from [25].

| Sun | | IRAS 20508 + 2011 | | | | |
|-----|--------------------|-----------------------|--------------------|-----|----------|------------------|
| | | 4800 K, 1.5, 4.0 km/s | | | | |
| E | $\log \epsilon(E)$ | X | $\log \epsilon(X)$ | n | σ | $[X/Fe]_{\odot}$ |
| C | 8.55 | CI | <i>9.07</i> | 4 | 0.24 | +0.88 |
| N | 7.97 | NI | <i>9.33</i> | 1 | | +1.72 |
| O | 8.87 | OI | 10.30 | 3 | 0.22 | +1.79 |
| Na | 6.33 | NaI | 6.55 | 4 | 0.30 | +0.58 |
| Mg | 7.58 | MgI | 6.87 | 3 | 0.20 | −0.35 |
| Al | 6.47 | AlI | 6.43 | 3 | 0.11 | +0.32 |
| Si | 7.55 | SiI | 7.27 | 14 | 0.20 | +0.08 |
| | | SiII | <i>7.52</i> | 1 | | +0.33 |
| S | 7.21 | Si | 7.59 | 5 | 0.37 | +0.74 |
| Ca | 6.36 | CaI | 6.04 | 18 | 0.22 | +0.04 |
| Sc | 3.17 | ScII | 2.59 | 7 | 0.21 | −0.20 |
| Ti | 5.02 | TiI | 4.51 | 35 | 0.21 | −0.15 |
| | | TiII | 4.38 | 8 | 0.25 | −0.28 |
| V | 4.00 | VI | 3.50 | 17 | 0.28 | −0.14 |
| | | VII | 3.60 | 3 | 0.21 | −0.04 |
| Cr | 5.67 | CrI | 5.54 | 16 | 0.18 | +0.23 |
| | | CrII | 5.41 | 6 | 0.32 | +0.10 |
| Mn | 5.39 | MnI | 4.81 | 12 | 0.30 | −0.22 |
| Fe | 7.50 | FeI | 7.11 | 138 | 0.23 | +0.03 |
| | | FeII | 7.16 | 15 | 0.24 | −0.02 |
| Co | 4.92 | CoI | 4.66 | 10 | 0.26 | +0.10 |
| Ni | 6.25 | NiI | 5.61 | 21 | 0.19 | −0.28 |
| Cu | 4.21 | CuI | 3.62 | 2 | | −0.23 |
| Zn | 4.60 | ZnI | 4.00 | 2 | | −0.24 |
| Y | 2.24 | YI | 1.70 | 4 | 0.35 | −0.18 |
| | | YII | 1.62 | 4 | 0.25 | −0.26 |
| Zr | 2.60 | ZrI | 1.57 | 2 | | −0.67 |
| Ba | 2.13 | BaII | 1.32 | 1 | | −0.45 |
| | | | 1.40 | 3 | 0.19 | −0.37 |
| La | 1.22 | LaII | 0.79 | 3 | 0.25 | −0.07 |
| Ce | 1.55 | CeII | 0.96 | 3 | 0.28 | −0.28 |
| Pr | 0.71 | PrII | 0.25 | 2 | | −0.10 |
| Nd | 1.50 | NdII | 1.15 | 7 | 0.22 | +0.01 |
| Eu | 0.51 | EuII | 0.08 | 2 | | −0.07 |